

1 FtsW exhibits distinct processive movements driven by either septal cell  
2 wall synthesis or FtsZ treadmilling in *E. coli*

3 Xinxing Yang<sup>1</sup>, Ryan McQuillen<sup>1</sup>, Zhixin Lyu<sup>1</sup>, Polly Phillips-Mason<sup>2</sup>, Ana De La Cruz<sup>1</sup>, Joshua W.  
4 McCausland<sup>1</sup>, Hai Liang<sup>3,5</sup>, Kristen E. DeMeester<sup>3</sup>, Catherine L. Grimes<sup>3,4</sup>, Piet de Boer<sup>2\*</sup>, Jie Xiao<sup>1\*</sup>

5

6 <sup>1</sup>Department of Biophysics and Biophysical Chemistry, Johns Hopkins School of Medicine, Baltimore,  
7 Maryland, 21205, USA.

8 <sup>2</sup>Department of Molecular Biology & Microbiology, School of Medicine, Case Western Reserve  
9 University, Cleveland, Ohio 44106-4960, USA.

10 <sup>3</sup>Department of Chemistry and Biochemistry, University of Delaware, 134 Brown Lab, Newark, Delaware  
11 19716, USA.

12 <sup>4</sup>Department of Biological Sciences, University of Delaware, Newark, Delaware 19716, USA.

13 <sup>5</sup>Current address: Dermatology Branch, National Institute of Arthritis and Musculoskeletal and Skin  
14 Diseases, NIH, Bethesda, MD 20892, USA

15 \*Correspondence and requests for materials should be addressed to P.d.B. (email: pad5@case.edu) and  
16 J.X. (email: xiao@jhmi.edu)

17 **Abstract**

18        During bacterial cell division, synthesis of new septal peptidoglycan (sPG) is crucial for  
19    successful cytokinesis and cell pole morphogenesis. FtsW, a SEDS (Shape, Elongation, Division and  
20    Sporulation) family protein and an indispensable component of the cell division machinery in all  
21    walled bacterial species, was recently identified *in vitro* as a new monofunctional peptidoglycan  
22    glycosyltransferases (PGTase). FtsW and its cognate monofunctional transpeptidase (TPase) class b  
23    penicillin binding protein (PBP3 or FtsI in *E. coli*) may constitute the essential, bifunctional sPG  
24    synthase specific for new sPG synthesis. Despite its importance, the septal PGTase activity of FtsW  
25    has not been documented *in vivo*. How its activity is spatiotemporally regulated *in vivo* has also  
26    remained unknown. Here we investigated the septal PGTase activity and dynamics of FtsW in *E.*  
27    *coli* cells using a combination of single-molecule imaging and genetic manipulations. We showed  
28    that FtsW exhibited robust activity to incorporate an *N*-acetylmuramic acid analog at septa in the  
29    absence of other known PGTases, confirming FtsW as the essential septum-specific PGTase *in vivo*.  
30    Furthermore, we identified two populations of processively moving FtsW molecules at septa. A fast-  
31    moving population is driven by the treadmilling dynamics of FtsZ and independent of sPG  
32    synthesis. A slow-moving population is driven by active sPG synthesis and independent of FtsZ  
33    treadmilling dynamics. We further identified that FtsN, a potential sPG synthesis activator, plays  
34    an important role in promoting the slow-moving, sPG synthesis-dependent population. Our results  
35    support a two-track model, in which inactive sPG synthase molecules follow the fast treadmilling  
36    “Z-track” to be distributed along the septum; FtsN promotes their release from the “Z-track” to  
37    become active in sPG synthesis on the slow “sPG-track”. This model integrates spatial information  
38    into the regulation of sPG synthesis activity and could serve as a mechanism for the spatiotemporal  
39    coordination of bacterial cell wall constriction.

40        To investigate the role of FtsW in sPG synthesis *in vivo*, we employed a cysteine-modification  
41    inactivation assay<sup>1,2</sup>. Based on the homology structure of RodA<sup>3</sup>, we generated twelve *ftsW*<sup>C</sup> alleles that

42 each encodes a unique cysteine residue on the periplasmic side of FtsW (Extended Data Fig. 1 and  
43 Supplementary Table 1). Amongst these, we identified FtsW<sup>I302C</sup> as a promising candidate for *in vivo*  
44 inactivation with the cysteine-reactive reagent MTSES (2-sulfonatoethyl methanethiosulfonate)<sup>4</sup>. Cells  
45 expressing FtsW<sup>I302C</sup> from the native chromosomal *ftsW* locus grew with a wild-type (WT)-like doubling  
46 time and cell morphology in the absence of MTSES but grew into long chains and stopped dividing when  
47 treated with MTSES (Extended Data Fig. 2, Supplementary Movie 1, 2). WT parental BW25113 cells  
48 treated with MTSES did not show any appreciable cell division defect (Extended Data Fig. 2), indicating  
49 that MTSES specifically inhibited the essential function of FtsW<sup>I302C</sup>. The homology structure of FtsW  
50 indicates that I302 resides in the periplasmic loop 4 between transmembrane helices 7 and 8, likely near  
51 critical residues of the PGTase activity of SEDS proteins<sup>3,5</sup>.

52 To probe the contribution of FtsW to sPG synthesis *in vivo*, we labeled new cell wall  
53 peptidoglycan (PG) synthesis using an alkyne-modified N-acetylmuramic acid (alkyne-NAM). Unlike  
54 fluorescent D-amino acid (FDAA) labels, which are incorporated into the peptide stem of *E. coli* PG  
55 through periplasmic exchange reactions<sup>6</sup>, alkyne-NAM enters the endogenous cytoplasmic PG  
56 biosynthetic pathway and incorporates into newly linked glycan chains<sup>7</sup> composed of alternating units of  
57 NAM and *N*-acetylglucosamine (NAG). Subsequent labeling of the alkyne using a fluorophore-  
58 conjugated azide by copper catalyzed azide-alkyne cycloaddition (CuAAC) also known as “CLICK”  
59 chemistry allows for visualization and quantification of newly polymerized glycan strands<sup>8</sup>.

60 In WT cells treated with or without MTSES, we observed robust NAM labeling (2 mg/ml, 30 min,  
61 Fig. 1a, Methods) at septa. In *ftsW*<sup>I302C</sup> cells treated with MTSES (1 mM, 30 min), we observed a  
62 significant reduction in the percentage of cells showing septal labeling above the background level (from  
63 34 ± 4% to 22 ± 4%,  $\mu \pm$  S.E.M., N > 300 cells, three independent repeats, Fig. 1b, orange bars,  
64 Supplementary Table 3). Furthermore, in this septal-labeled population of MTSES-treated *ftsW*<sup>I302C</sup> cells,  
65 the median fluorescence intensity dropped to 70 ± 4% compared to that in untreated cells (Extended Data  
66 Fig. 3, Supplementary Table 3). Thus, inhibition of FtsW<sup>I302C</sup> activity by MTSES caused a total reduction

67 in septal NAM labeling of ~ 55% (100% – 22% / 34% × 70%, Fig. 1c, orange bar), consistent with a  
68 major role of FtsW in septal glycan chain polymerization. The fact that significant NAM incorporation  
69 still occurred at septa of MTSES-treated *ftsW*<sup>I302C</sup> cells is consistent with the previous report showing that  
70 FtsW is not an essential lipid II flippase acting upstream of sPG synthesis<sup>9</sup> and that other PGTases  
71 contribute to septal morphogenesis as well<sup>10</sup>. The inability of MTSES-treated *ftsW*<sup>I302C</sup> cells to complete  
72 cell division, even when other PGTases are still active, highlights the essential role of FtsW in successful  
73 cell wall constriction.

74 To further investigate the relative contributions to sPG polymerization by FtsW and other  
75 relevant PGTases in *E. coli*, we introduced the chromosomal *ftsW*<sup>I302C</sup> allele into a  $\Delta 3$  *ponB*<sup>S247C</sup> strain  
76 background<sup>1</sup> to create a  $\Delta 3$  *ponB*<sup>S247C</sup> *ftsW*<sup>I302C</sup> strain. The  $\Delta 3$  *ponB*<sup>S247C</sup> strain lacks the genes for PBP1A,  
77 PBP1C and MtgA, and expresses a variant (S247C) of PBP1B (PBP1B<sup>S247C</sup>, encoded by *ponB*<sup>S247C</sup>) that,  
78 like FtsW<sup>I302C</sup>, can be inactivated by exposure to MTSES. Untreated  $\Delta 3$  *ponB*<sup>S247C</sup> cells exhibited a similar  
79 percentage of labeled septa as WT cells (32 ± 1%,  $\mu \pm$  S.E.M., N > 300 cells, three independent repeats,  
80 Fig. 1b, blue bar, Supplementary Table 3), indicating that PBP1A, PBP1C and MtgA together contribute  
81 minimally to the essential sPG polymerization activity under our experimental condition. When the  
82 PGTase activity of PBP1B<sup>S247C</sup> in  $\Delta 3$  *ponB*<sup>S247C</sup> cells was inhibited by MTSES, the percentage of labeled  
83 septa dropped to 14 ± 3 % with the median intensity reduced to 65 ± 12 % of the WT MTSES-treated  
84 level (Fig. 1b, blue bar, Supplementary Table 3), corresponding to a total loss of septal labeling of ~ 72 %  
85 (100% – 14% / 32% × 65% Fig. 1c, blue bar). Simultaneous inactivation of PBP1B and FtsW by MTSES  
86 in  $\Delta 3$  *ponB*<sup>S247C</sup> *ftsW*<sup>I302C</sup> cells, however, led to a background level of septal NAM labeling  
87 indistinguishable from that when the essential Lipid II flippase MurJ<sup>9</sup> was inhibited (Fig. 1b, c, compare  
88 purple and gray bars, Supplementary Table 3). These results strongly support that FtsW and PBP1B are  
89 the two major septal PGTases, and that FtsW is the only essential septum-specific monofunctional  
90 PGTase.

91        Previously, we and others showed that FtsZ's treadmilling dynamics drive the processive  
92    movement of FtsW's cognate TPase (FtsI in *E. coli* and PBP2B in *B. subtilis*) at septa<sup>11,12</sup>. Such FtsZ-  
93    dependent dynamics were proposed to direct the spatial distribution of sPG synthesis complexes and play  
94    an important role in septum morphogenesis<sup>11,12</sup>. Because a large body of biochemical and genetic studies  
95    indicates that FtsW associates with FtsI to form a bifunctional sPG synthase complex<sup>13-15</sup>, we investigated  
96    whether FtsW exhibited similar processive movement at septa using single molecule tracking (SMT).

97        We constructed a C-terminal fusion of FtsW with the red fluorescent protein TagRFP-t  
98    (Supplementary Table 1) and will refer to the fusion protein as FtsW-RFP for simplicity. We verified that  
99    upon replacement of chromosomal *ftsW* with the *ftsW-rfp* allele (strain JXY422), FtsW-RFP localizes  
100   correctly to midcell and supports normal cell division under our experimental conditions (Extended data  
101   Fig. 2). To enable single-molecule detection, we expressed FtsW-RFP ectopically at a low level (plasmid  
102   pXY349) in the presence of WT FtsW in BW25113 cells. We tracked the dynamics of single FtsW-RFP  
103   molecules at midcell with a frame rate of 2 Hz using wide-field fluorescence microscopy. This slow  
104   frame rate allowed us to focus on septum-localized FtsW-RFP molecules by effectively filtering out fast,  
105   randomly diffusing molecules along the cylindrical part of the cell body. Using a custom-developed  
106   unwrapping algorithm (Extended Data Fig. 4, Methods), we decomposed two-dimensional (2D)  
107   trajectories of individual FtsW-RFP molecules obtained from the curved cell surfaces at midcell to one-  
108   dimensional (1D) trajectories along the circumference and long axis of the cell respectively (Fig. 2,  
109   Extended Data Fig. 4, Methods).

110        We found that single FtsW-RFP molecules displayed heterogenous dynamics at midcell. Some  
111   FtsW-RFP molecules were relatively stationary and confined to small regions (Fig. 2a-c, Supplementary  
112   Movie 3), some moved processively along the cell circumference (Fig. 2d-f, Supplementary Movie 4),  
113   and many dynamically transitioned between these states (Fig. 2g-i, Extended Data Fig. 5, Supplementary  
114   Movie 5-9). To quantitatively identify different movements and corresponding speeds, we split each  
115   trajectory into multiple segments and identified each as stationary or directional movement based on the

116 corresponding displacement along the midcell circumference (Methods). Segments of directional  
117 movement were fit to a straight line to extract the directional moving speed  $v$  (Fig. 2e, h, Extended Data  
118 Fig. 5, Methods). We quantified that, on average, a FtsW-RFP molecule was stationary for about half the  
119 time ( $51\% \pm 2\%$ ,  $\mu \pm \text{S.E.M.}$ ,  $D = 0.0019 \mu\text{m}^2/\text{s}$ , from 695 trajectories), and spent the other half time  
120 moving processively along the midcell circumference (Supplementary Table 4).

121 Notably, the speeds of all directionally moving FtsW-RFP molecules showed a much wider  
122 distribution (Fig. 2j, second panel and k;  $\mu \pm \text{s.d.}$  at  $23 \pm 30 \text{ nm/s}$ ,  $n = 320$  segments) and displayed an  
123 additional slow-moving peak (Fig. 2j, second panel, green curve) when compared to the distribution of  
124 FtsZ's treadmilling speed<sup>11</sup> (Fig. 2j, top panel, blue curve). The corresponding cumulative probability  
125 density function (CDF) of FtsW-RFP's speed distribution was best fit by the sum of two populations, one  
126 fast and one slow, instead of one single fast population as that for the FtsZ treadmilling speed distribution  
127 (Fig. 2l, Extended Data Fig. 6a). The fast-moving population ( $\sim 64 \pm 16\%$ ,  $\mu \pm \text{S.E.M.}$ ,  $n = 320$  segments)  
128 of FtsW-RFP displayed a mean speed of  $30 \pm 3 \text{ nm/s}$ , ( $\mu \pm \text{S.E.M.}$ , Fig. 2j, second panel, red curve,  
129 Supplementary Table 4), similar to the average FtsZ treadmilling speed we previously measured<sup>11</sup> ( $28 \pm 1$   
130  $\text{nm/s}$ ,  $\mu \pm \text{S.E.M.}$ ). The slow-moving population ( $\sim 36 \pm 16\%$ ,  $\mu \pm \text{S.E.M.}$ ) of FtsW-RFP molecules had  
131 an average speed of  $\sim 8 \text{ nm/s}$  ( $8 \pm 1 \text{ nm/s}$ , Fig. 2j, top, green curve, Supplementary Table 4). The presence  
132 of, and transition between, the two different types of directional movements could also be directly  
133 observed in many individual FtsW-RFP trajectories (Fig. 2h, Extended Data Fig. 5).

134 To investigate how the two directionally moving populations respond to FtsZ's treadmilling  
135 dynamics, we performed SMT of FtsW-RFP in five strains with mutations that affect FtsZ GTPase  
136 activity ( $ftsZ^{E238A}$ ,  $ftsZ^{E250A}$ ,  $ftsZ^{D269A}$ ,  $ftsZ^{G105S}$  and  $ftsZ^{D158A}$ ). We previously showed that in these strains  
137 the average directional moving speed of FtsI responds linearly to reduced FtsZ treadmilling speed with  
138 decreasing GTPase activity<sup>11</sup>. Here we found that in these FtsZ GTPase mutant backgrounds the average  
139 speed of all moving FtsW-RFP molecules correlated linearly with FtsZ's treadmilling speed in a nearly

140 identical manner as what we previously observed for FtsI (Fig. 2k), suggesting that FtsW moves together  
141 with FtsI in a sPG synthase complex as expected<sup>13-15</sup>.

142 Most interestingly, close inspection and CDF analysis of the two moving populations of FtsW-  
143 RFP in FtsZ GTPase mutants (Fig. 2j, l) revealed that the reduction of the average speed of all moving  
144 FtsW-RFP molecules was primarily caused by reduced speeds of the fast-moving populations, whereas  
145 the slow-moving populations maintained a relatively constant speed (Fig. 2m, Extended Data Fig. 6,  
146 Supplementary Table 4). The differential responses of the two moving FtsW populations to FtsZ  
147 treadmilling dynamics suggest that the fast-moving population is driven by FtsZ treadmilling dynamics,  
148 while the slow-moving population is not. Note that a recent study showed that in *S. pneumoniae* the  
149 FtsW-PBP2x pair only exhibited one single directional moving population that is FtsZ-independent<sup>16</sup>.

150 Additionally, we observed that on average FtsW-RFP spent more time in the stationary state as  
151 FtsZ GTPase activity decreased (Extended Data Fig. 7a, Supplementary Table 4). Speed distributions  
152 immediately before and after stationary interludes also shifted significantly to high speeds (Extended Data  
153 Fig. 7b). Given that the total sPG synthesis activity is not affected in these FtsZ GTPase mutants<sup>11,17</sup>, and  
154 that FtsW or FtsI could track the shrinking end of a treadmilling FtsZ filament through a Brownian  
155 Rachet mechanism (our unpublished data), these observations indicate that stationary FtsW-RFP  
156 molecules are likely the ones immobilized in the middle of FtsZ filaments before it starts to track or after  
157 it dissociates from a treadmilling FtsZ filament. The increased time FtsW-RFP molecules spent in the  
158 stationary state in these FtsZ GTPase mutants likely reflects the increased time it takes for the end of a  
159 treadmilling FtsZ polymer with a reduced speed to come across a stationary FtsW-RFP molecule to  
160 mobilize it under these experimental conditions.

161 In *E. coli*, the cell wall constriction rate is not limited by FtsZ treadmilling speed but dependent  
162 on sPG synthesis activity<sup>11,17</sup>. Therefore, it is unlikely that the FtsZ-dependent, fast-moving FtsW  
163 molecules are active in sPG synthesis. Rather, the FtsZ-independent population could represent

164 catalytically active molecules with their slow speed reflecting processive sPG synthesis. To examine this  
165 possibility, we tracked FtsW-RFP molecules under conditions of altered sPG synthesis activity.

166 We first tracked the movement of FtsW<sup>I302C</sup>-RFP molecules in the BW25113 *ftsW*<sup>I302C</sup>  
167 background (JXY559/pAD004) in the absence and presence of MTSES. In the absence of MTSES, we  
168 again observed two directionally moving populations of FtsW<sup>I302C</sup>-RFP, one fast at  $37 \pm 9$  nm/s and one  
169 slow at  $10 \pm 1$  nm/s (average speed at  $22 \pm 2$  nm/s,  $\mu \pm$  s.e.m.,  $N = 169$  segments, Fig. 3a, b, black,  
170 Supplementary Table 5). In the presence of MTSES, the slow-moving population of FtsW<sup>I302C</sup>-RFP was  
171 significantly depleted, as indicated by the right-shifted (higher speed) CDF curve, which can be well fit  
172 by a single moving population with an average speed of  $26 \pm 2$  nm/s ( $\mu \pm$  s.e.m.,  $N = 272$  segments, Fig.  
173 3a, b, lime, Extended Data Fig. 8, Supplementary Table 5). Since MTSES specifically blocks FtsW<sup>I302C</sup>-  
174 dependent sPG synthesis (Fig. 1), these results support the hypothesis that the slow-moving FtsW-RFP  
175 molecules represent the catalytically active form of FtsW.

176 To further confirm the correlation between sPG synthesis activity and the slow-moving  
177 population of FtsW-RFP, we used cells with a superfission (SF) allele of *ftsW* (*ftsW*<sup>E289G</sup>) that confers a  
178 short-cell phenotype and alleviates the need for FtsN, an otherwise essential positive regulator of sPG  
179 synthesis (Extended Data Fig. 9). SMT of FtsW<sup>E289G</sup>-RFP in *ftsW*<sup>E289G</sup> cells again revealed one fast- and  
180 one slow-moving population (Fig 3a, dark green histogram), and the corresponding CDF curve shifted  
181 significantly to the left (lower speeds) compared to that of FtsW-RFP in the parental WT TB28  
182 background (Fig. 3a, gray histogram, and Fig. 3b, gray curve). Accordingly, the average speed of all  
183 directional moving FtsW<sup>E289G</sup>-RFP molecules in *ftsW*<sup>E289G</sup> cells was significantly lower than that of FtsW-  
184 RFP in WT cells ( $14 \pm 1$  vs  $18 \pm 2$  nm/s, Supplemental Table 5). These results are consistent with the  
185 hypothesis that the slow-moving population of FtsW is coupled to sPG synthesis activity.

186 Next, as FtsW and FtsI likely form a bifunctional sPG synthase complex and move together as we  
187 showed above, inhibiting the crosslinking activity of FtsI might stall the FtsWI complex and reduce the

188 slow-moving, sPG synthesis-dependent population of FtsW. To examine this possibility, we specifically  
189 inhibited the TPase activity of FtsI using aztreonam (50  $\mu$ g/ml, 30 min). We found that the distribution of  
190 directional moving speed of FtsW-RFP (Fig. 3c, purple) and the corresponding CDF curve (Fig. 3d,  
191 purple) shifted significantly to the right (faster speed) and was best fit by a single population with an  
192 average speed of  $26 \pm 2$  nm/s ( $\mu \pm$  s.e.m.,  $N = 238$ , Extended Data Fig. 8, Supplemental Table 5), similar  
193 to that in the FtsW<sup>1302C</sup>-inhibited condition (Fig. 3a, b) and the treadmilling speed of FtsZ (Fig. 11).

194 In contrast to what was observed in the FtsI-inhibited condition, we observed the opposite trend  
195 in the movement of FtsW-RFP in cells expressing a superfission variant of FtsI (FtsI<sup>S167I</sup>). FtsI<sup>S167I</sup> is  
196 similar to FtsW<sup>E289G</sup> in alleviating the essentiality of FtsN but does so only partially (Extended Data Fig.  
197 9). In *ftsI*<sup>S167I</sup> cells, a major population of FtsW-RFP ( $72\% \pm 7\%$ ,  $N = 254$  segments) moved at  $6.0 \pm 0.2$   
198 nm/s and a minor population moved at  $19 \pm 7$  nm/s (Fig. 3c, d, red Supplementary Table 5). The resulting  
199 CDF curve also shifted significantly to the left (lower speed, Fig. 3d, red) compared to that of the WT  
200 parental strain (Fig. 3d, gray). These results are again consistent with the hypothesis that the slow-moving  
201 population is driven by sPG synthesis activity.

202 In *E. coli* under balanced growth, the cellular level of PG synthesis precursors limits cell growth  
203 and cell wall constriction rates<sup>18,19</sup>. Therefore, we reasoned that the slow-moving population of FtsW  
204 could also be modulated by the level of available PG precursors. To examine this possibility, we  
205 increased the PG precursor level by growing cells in a rich defined medium (EZRDM), which we  
206 previously showed to increase the cell wall constriction rate two-fold compared that in minimal M9  
207 medium<sup>17</sup>. We found that the slow-moving population ( $11.0 \pm 0.3$  nm/s,  $\mu \pm$  s.e.m.,  $N = 894$  segments,  
208 Fig. 3e, f, yellow) increased from  $36\% \pm 16\%$  in M9 to  $52\% \pm 4\%$  in EZRDM, and the remaining fast-  
209 moving population in EZRDM displayed similar speed ( $29 \pm 3$  nm/s,  $\mu \pm$  s.e.m., Fig. 3e, f, yellow,  
210 Supplemental Table 5) as in M9. In contrast, when cells were treated with Fosfomycin to inactivate MurA,  
211 the first essential enzyme towards synthesis of uridine diphosphate *N*-acetyl muramic acid(UDP-NAM)  
212 and Lipid II<sup>20</sup>, the slow-moving (8 – 10 nm/s) population of FtsW-RFP molecules was drastically

213 diminished, while the population moving at the speed of FtsZ treadmilling (average speed at  $25 \pm 10$  nm/s,  
214  $N = 138$  segments) persisted (Fig. 3e, f, orange, Extended Data Fig. 8, Supplementary Table 5).  
215 Additionally, we observed a population of FtsW-RFP molecules that moved even faster (average speed at  
216  $63 \pm 14$  nm/s,  $N = 138$  segments, Supplementary Table 5). Why the latter population appeared is unclear,  
217 but it is conceivable that Fosfomycin-induced loss of overall cell wall integrity increases the number of  
218 very fast moving diffusive FtsW-RFP molecules that can be misinterpreted by the SMT algorithm as  
219 moving directionally.

220 In all the experiments described above, the slow-moving population of FtsW-RFP became  
221 depleted when sPG synthesis activity was reduced or abolished, but the population rather increased when  
222 sPG synthesis activity was enhanced. Additionally, the fraction of time a FtsW-RFP molecule spent in the  
223 stationary state correlated inversely with sPG synthesis activity: high sPG synthesis activity correlated  
224 with less time spent in stationary state and low sPG synthesis activity correlated with more time in  
225 stationary state (Fig. 3g, Supplemental Table 5),

226 Our results so far demonstrated that two directionally moving populations of FtsW exist *in vivo*.  
227 The fast-moving population is most likely driven by FtsZ treadmilling dynamics but inactive in sPG  
228 synthesis, whereas the slow-moving population is most likely active and driven by sPG synthesis. The  
229 presence of active and inactive FtsW populations brought up an interesting question: what determines the  
230 partitioning of the two populations? Previous studies in *E. coli* have shown that when FtsW and FtsI are  
231 first recruited to the division site by a complex of the FtsB, FtsL and FtsQ proteins (FtsBLQ), they are  
232 kept in an inactive state by the complex and cannot initiate sPG synthesis until FtsN, the last essential  
233 division protein to accumulate at the site, relieves the inhibitory effect of FtsQLB<sup>21,22</sup>. Therefore, FtsN  
234 may play an important role in triggering the transition of FtsW from the fast-moving (FtsZ-dependent) to  
235 slow-moving (sPG synthesis-dependent) state.

236 To test this hypothesis, we used an FtsN-depletion strain (EC1908)<sup>23</sup> wherein chromosomal *ftsN*  
237 is controlled by the *araBAD* regulatory region, and which grows and divides normally in the presence of

238 0.2% of arabinose (Extended Data Fig. 11, Supplementary Table 1). After overnight growth (~15 hours)  
239 in M9 medium without arabinose, the average cellular FtsN level was depleted to ~ 44% of that in WT  
240 type cells (Extended Data Fig. 11) and many cells grew into long filaments with shallow constrictions  
241 (Fig. 4a). We then tracked FtsW-RFP molecules at shallow constriction sites in these filamentous cells.  
242 Similar to the trend we observed above, there was a significant increase in the fraction of time FtsW-RFP  
243 stayed stationary ( $80 \pm 2\%$ ) compared to WT cells ( $51 \pm 2\%$ , Supplementary Table 5). Most importantly,  
244 the slow-moving population of FtsW-RFP was drastically eliminated, and the remaining moving FtsW-  
245 RFP molecules moved at an average speed similar to FtsZ treadmilling (Fig. 4b, c, blue, Supplementary  
246 Table 5).

247 Next, to assess the effects of FtsN on FtsW dynamics under conditions where FtsN is no longer  
248 essential, we tracked the movements of FtsW-RFP in a *ftsB<sup>E56A</sup>* superfission strain (BL167) that still  
249 produces FtsN, and also in strain BL173 (*ftsB<sup>E56</sup> ΔftsN*) that lacks FtsN completely. The *ftsB<sup>E56A</sup>*  
250 superfission allele causes cells to initiate sPG synthesis earlier in the division cycle than normal, leading  
251 to a small-cell phenotype<sup>21</sup>. While it also allows cells to grow and divide in the complete absence of FtsN,  
252 *ftsB<sup>E56A</sup> ΔftsN* cells divide less efficiently than wt and are modestly elongated<sup>21</sup> (Supplementary Table 6).  
253 In *ftsB<sup>E56A</sup>* cells, we observed a significantly increased slow-moving population of FtsW (Fig. 4b, orange);  
254 the fast-moving, FtsZ-dependent population of FtsW-RFP was essentially abolished, and nearly all ( $90 \pm$   
255 1%) directional moving FtsW-RFP molecules moved at an average speed of ~ 10 nm/s ( $10 \pm 1$  nm, Fig.  
256 4b, c, orange, Supplementary Table 5). Most interestingly and as we expected, in *ftsB<sup>E56A</sup> ΔftsN* cells  
257 where FtsN is absent, the slow-moving population of FtsW-RFP was reduced while the fast-moving  
258 population recovered to approximately the same level as that in WT cells (Fig 4b,c, yellow,  
259 Supplementary Table 5). These results demonstrated that even though FtsN is no longer essential in the  
260 superfission *ftsB<sup>E56A</sup>* background, it still contributes to the transitioning of FtsW from the fast-moving,  
261 FtsZ-dependent state to the slow-moving, sPG synthesis-dependent mode.

262 To summarize our observations in this work, in Fig. 5a we plotted and sorted from low to high the  
263 average speeds of all directionally moving FtsW-RFP molecules under conditions where sPG synthesis  
264 activity was altered. We observed a clear anti-correlation of the average directional moving speed of  
265 FtsW with expected sPG synthesis activity qualitatively: FtsW moves fast when sPG synthesis activity  
266 was reduced or abolished, and slowly when sPG synthesis activity was elevated (Fig. 5a), due to the  
267 partitioning of FtsW between the fast-moving, FtsZ-dependent population and the slow-moving, sPG-  
268 dependent population (Extended Data Fig. 12a). Additionally, the fraction of time FtsW spent in the  
269 stationary state anti-correlated with sPG synthesis activity: FtsW spent more time in the stationary state  
270 when sPG synthesis was reduced or abolished, and less time when sPG synthesis activity was elevated  
271 (Extended Data Fig. 12b). Notably, a recent study showed that the directional movement of PBP2 (the  
272 counterpart of FtsI in cell wall elongation machinery in *E. coli*) also depends on the cell wall synthesis  
273 activity but not the cytoskeleton protein MreB<sup>24</sup>.

274 Taken together, our data support a two-track model (Fig. 5b), in which FtsW, and most likely FtsI  
275 and possibly other sPG remodeling enzymes and regulators as well, occupy at least two 'tracks' within the  
276 septum: a fast 'Z-track' representing inactive molecules associated with treadmilling FtsZ polymers, and a  
277 slower 'sPG-track' representing active molecules that exited the Z-track to produce sPG processively.  
278 Some of these molecules could also remain stationary when they are not mobilized by either one of the  
279 tracks. FtsN promotes the release of inactive sPG synthase from treadmilling FtsZ polymers to pursue the  
280 sPG-track for active synthesis. In this scenario, FtsWI may associate with the suppression complex  
281 FtsBLQ on the Z-track in an inactive state, and switch to associate with the activator FtsN on the sPG  
282 track to become active. Further investigations to examine the dynamics of the FtsQLB and FtsN will help  
283 elucidate these possibilities. This two-track model integrates spatial information into the regulation of  
284 sPG synthesis activity and could serve as a novel mechanism for the spatiotemporal coordination of  
285 bacterial cell wall constriction.

286 **Acknowledgements**

287 The authors thank lab members in the Xiao and de Boer labs for helpful discussions and technical  
288 assistance, Dr. G. Hauk for sharing plasmids and the CRISPR-Cas9/λ-red recombineering cloning method,  
289 Dr. D. S. Weiss for the EC1908 strain, pDSW406 plasmid, anti-FtsN serum, and helpful suggestions on  
290 FtsW immunoblot, Dr. T. Berhardt for HC532 strain, Dr. E. Goley for the help on cell growth  
291 measurement. Dr. R. Tsien for the TagRFP-T construct. This work was supported by NIH R01 GM57059  
292 (to P.d.B), NIH R01 GM086447 (to J.X.), GM125656 (subcontract to J.X.), NSF EAGER Award MCB-  
293 1019000 (to J.X.), and a Hamilton Smith Innovative Research Award (to J.X.)

294 **Reference:**

295 1. Cho, H. *et al.* Bacterial cell wall biogenesis is mediated by SEDS and PBP polymerase families  
296 functioning semi-autonomously. *Nat Microbiol* **1**, 16172 (2016).

297 2. Butler, E. K., Davis, R. M., Bari, V., Nicholson, P. A. & Ruiz, N. Structure-function analysis of MurJ  
298 reveals a solvent-exposed cavity containing residues essential for peptidoglycan biogenesis in *Escherichia*  
299 *coli*. *J Bacteriol* **195**, 4639–4649 (2013).

300 3. Sjödt, M. *et al.* Structure of the peptidoglycan polymerase RodA resolved by evolutionary coupling  
301 analysis. *Nature* **556**, 118–121 (2018).

302 4. Karlin, A. & Akbas, M. H. Substituted-cysteine accessibility method. *Meth Enzymol* **293**, 123–145  
303 (1998).

304 5. Meeske, A. J. *et al.* SEDS proteins are a widespread family of bacterial cell wall polymerases. *Nature*  
305 **537**, 634–638 (2016).

306 6. Kuru, E. *et al.* In Situ probing of newly synthesized peptidoglycan in live bacteria with fluorescent D-  
307 amino acids. *Angew Chem Int Ed Engl* **51**, 12519–12523 (2012).

308 7. Liang, H. *et al.* Metabolic labelling of the carbohydrate core in bacterial peptidoglycan and its  
309 applications. *Nat Commun* **8**, 15015 (2017).

310 8. Kolb, H. C., Finn, M. G. & Sharpless, K. B. Click Chemistry: Diverse Chemical Function from a Few  
311 Good Reactions. *Angew Chem Int Ed Engl* **40**, 2004–2021 (2001).

312 9. Sham, L.-T. *et al.* MurJ is the flippase of lipid-linked precursors for peptidoglycan biogenesis. *Science*  
313 **345**, 220–222 (2014).

314 10. Egan, A. J. F. & Vollmer, W. The physiology of bacterial cell division. *Ann N Y Acad Sci* **1277**, 8–28  
315 (2012).

316 11. Yang, X. *et al.* GTPase activity-coupled treadmilling of the bacterial tubulin FtsZ organizes septal cell  
317 wall synthesis. *Science* **355**, 744–747 (2017).

318 12. Bisson-Filho, A. W. *et al.* Treadmilling by FtsZ filaments drives peptidoglycan synthesis and bacterial  
319 cell division. *Science* **355**, 739–743 (2017).

320 13. Di Lallo, G., Fagioli, M., Barionovi, D., Ghelardini, P. & Paolozzi, L. Use of a two-hybrid assay to  
321 study the assembly of a complex multicomponent protein machinery: bacterial septosome differentiation.  
322 *Microbiology (Reading, Engl)* **149**, 3353–3359 (2003).

323 14. Fraipont, C. *et al.* The integral membrane FtsW protein and peptidoglycan synthase PBP3 form a  
324 subcomplex in *Escherichia coli*. *Microbiology (Reading, Engl)* **157**, 251–259 (2010).

325 15. Karimova, G., Dautin, N. & Ladant, D. Interaction network among *Escherichia coli* membrane  
326 proteins involved in cell division as revealed by bacterial two-hybrid analysis. *J Bacteriol* **187**, 2233–  
327 2243 (2005).

328 16. Perez, A. J. *et al.* Movement dynamics of divisome proteins and PBP2x:FtsW in cells of  
329 *Streptococcus pneumoniae*. *Proc Natl Acad Sci USA* **116**, 3211–3220 (2019).

330 17. Coltharp, C., Buss, J., Plumer, T. M. & Xiao, J. Defining the rate-limiting processes of bacterial  
331 cytokinesis. *Proc Natl Acad Sci USA* **113**, E1044–53 (2016).

332 18. Lee, T. K. *et al.* A dynamically assembled cell wall synthesis machinery buffers cell growth. *Proc  
333 Natl Acad Sci USA* **111**, 4554–4559 (2014).

334 19. Rojas, E., Theriot, J. A. & Huang, K. C. Response of *Escherichia coli* growth rate to osmotic shock.  
335 *Proc Natl Acad Sci USA* **111**, 7807–7812 (2014).

336 20. Kahan, F. M., Kahan, J. S., Cassidy, P. J. & Kropp, H. The mechanism of action of fosfomycin  
337 (phosphonomycin). *Ann N Y Acad Sci* **235**, 364–386 (1974).

338 21. Liu, B., Persons, L., Lee, L. & de Boer, P. A. J. Roles for both FtsA and the FtsBLQ subcomplex in  
339 FtsN-stimulated cell constriction in *Escherichia coli*. *Mol Microbiol* **95**, 945–970 (2015).

340 22. Tsang, M. J., & Bernhardt, T. G. A role for the FtsQLB complex in cytokinetic ring activation  
341 revealed by an ftsL allele that accelerates division. *Mol Microbiol* **95**, 925–944 (2015).

342 23. Tarry, M. *et al.* The *Escherichia coli* cell division protein and model Tat substrate SufI (FtsP)  
343 localizes to the septal ring and has a multicopper oxidase-like structure. *J Mol Biol* **386**, 504–519 (2008).

344 24. Wollrab, E., Özbaykal, G., Vigouroux, A. & Cordier, B. Transpeptidase PBP2 governs initial  
345 localization and activity of major cell-wall synthesis machinery in *Escherichia coli*. *BioRxiv* 716407  
346 (2019).

347 **Figure Legends**

348

349 **Figure 1. FtsW is the only essential septum-specific monofunctional PGTase. a.** Representative  
350 images of *E. coli* cells of different strain backgrounds labeled with AF647-conjugated NAM in the  
351 absence or presence of MTSES. The contrast of each image is adjusted to allow optimized visualization  
352 of septal labeling especially for the  $\Delta 3$  *ponB*<sup>S247C</sup> *ftsW*<sup>I302C</sup> and *murJ*<sup>A29C</sup> + MTSES conditions. The  
353 absolute intensity is summarized in Supplementary Table 3. Scale bar: 1  $\mu$ m. **b.** Mean percentage of cells  
354 with septal NAM labeling above background level in the absence or presence of MTSES. **c.** Mean  
355 percentage of total loss in septal NAM intensity of the five strains due to MTSES. Error bars: S.E.M. of  
356 three experimental repeats (dots). Strains used were BW25113 (wt), JXY559 (*ftsW*<sup>I302C</sup>), HC532 ( $\Delta 3$   
357 *ponB*<sup>S247C</sup>), JXY564 ( $\Delta 3$  *ponB*<sup>S247C</sup> *ftsW*<sup>I302C</sup>), and JXY589 (*murJ*<sup>A29C</sup>), all carrying plasmid pBBR1-KU.

358

359 **Figure 2. FtsW exhibits two processively moving populations that are differentially dependent on**  
360 **FtsZ's treadmilling dynamics. a, d and g:** Representative maximum fluorescence intensity projection  
361 images with superimposed single molecule trajectories (time-colored from blue to red) of two stationary  
362 FtsW-RFP molecules (**a**), one processively moving FtsW-RFP molecule (**d**), and one moving FtsW-RFP  
363 molecule that transitioned between different directions and speeds (**g**) in BW25113/ pXY349 cells  
364 (outlined in yellow). The corresponding kymographs are shown on the right. **b, e and h:** Unwrapped one-  
365 dimensional (1d) positions of the corresponding FtsW-RFP molecule along the circumference (red) and  
366 long axis (gray) of the cell. Positions along the circumference were fit with one or multiple straight lines  
367 to measure directional moving speeds (black). Positions along the long axis of the cell were used to  
368 confirm that the molecule remained at midcell. **c, f and i:** 1d MSD (mean squared displacement) of the  
369 corresponding FtsW-RFP molecule along the circumference (red) and long axis (gray) of the cell. FtsW-  
370 RFP molecule showed highly confined sub-diffusive motions in **c** and directional movement with average  
371 speeds of 8.4 nm/s and 13.9 nm/s in **f** and **i** respectively. **j.** Speed distribution (bars) of all processively  
372 moving FtsW-RFP molecules in FtsZ WT and GTPase mutants. The treadmilling speed distribution of

373 FtsZ adapted from <sup>11</sup> (blue) and the decomposed fast-moving (red) and slow-moving (green) populations  
374 of FtsW-RFP in WT cells were shown for comparison. The dashed green and red lines mark the speeds at  
375 8 nm/s and 29 nm/s respectively for guide of eyes. **k**. Average speeds of all moving FtsW-RFP molecules  
376 (dark blue) correlated linearly with average FtsZ treadmilling speed, as previously also observed for FtsI  
377 (cyan)<sup>11</sup>. **l**. Cumulative distribution function (CDF, open circles) and the corresponding two-population  
378 fitting (solid curves) of the moving speed distribution of FtsW-RFP in FtsZ WT and GTPase mutants. The  
379 CDF and one-population fitting for FtsZ's treadmilling speed distribution (blue, far right) are shown for  
380 comparison. The two-population fitting results were used to plot the fast-moving (red) and slow-moving  
381 (green) populations in **j**. **m**. Average speeds of the slow- (green) and fast-moving (red) populations of  
382 FtsW-RFP obtained from CDF fitting in **j** v.s. FtsZ treadmilling speed in FtsZ GTPase mutant strains<sup>11</sup>.  
383

384 **Figure 3: The slow-moving population of FtsW increases with enhanced sPG synthesis activity and**  
385 **depletes with reduced sPG synthesis activity. a.** Histograms of directional moving speeds of FtsW<sup>I302C</sup>-  
386 RFP in JXY559 (*ftsW*<sup>I302C</sup>) in the absence (black) and presence (lime) of MTSES, FtsW-RFP in TB28  
387 (WT, gray), and the superfission variant FtsW<sup>E289G</sup>-RFP in the same background (strain PM17, *ftsW*<sup>E289G</sup>,  
388 dark green). Note clear shifts to higher speeds in the histogram of FtsW<sup>I302C</sup>-RFP with MTSES (lime) and  
389 to lower speeds in the histogram of FtsW<sup>E289G</sup>-RFP (dark green) compared to the corresponding WT  
390 histograms. Dashed green and red lines marks speeds at 8 nm/s and 29 nm/s respectively for guide of eyes.  
391 **b.** CDF (circles) of histograms in **a** and the corresponding best fits (solid curves). Note the left shift of a  
392 CDF corresponds to a slower speed with enhanced sPG synthesis activity and the right shift corresponds  
393 to a higher speed with reduced sPG synthesis activity. **c.** Histograms of directional moving speeds of  
394 FtsW-RFP in BW25113 (wt) without (black) or with aztreonam to inhibit FtsI (purple) and in the  
395 superfission variant PM6 (*ftsI*<sup>R167S</sup>, red). **d.** CDF (circles) of histograms in **c** and the corresponding best  
396 fits (solid curves). **e.** Histograms of directional moving speeds of FtsW-RFP in rich defined EZRD  
397 medium (yellow) and in Fosfomycin-treated cells (orange). **f.** CDF (circles) of histograms in **e** and the

398 corresponding best fits (solid curves). **g.** Percentage of time FtsW-RFP and its variants spent in stationary  
399 mode correlates inversely with expected sPG synthesis activity.

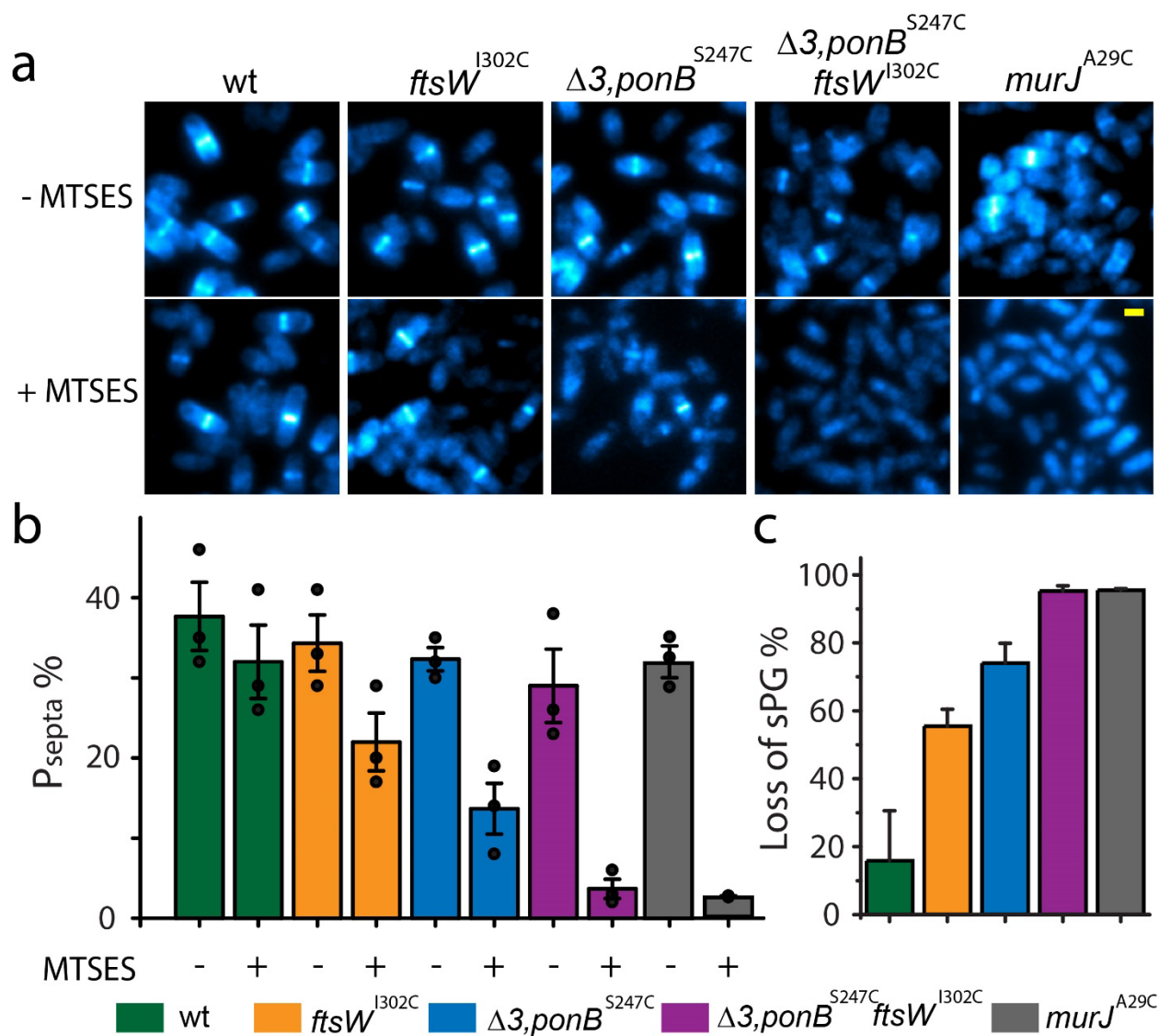
400

401 **Figure 4. FtsN plays an important role in promoting the slow-moving population of FtsW. a.** Bright-  
402 field images of WT (TB28), superfission  $ftsB^{E56A}$  (BL167),  $ftsB^{E56A} \Delta ftsN$  (BL173), and FtsN-depleted  
403 cells (EC1908). **b.** Histograms of directional moving speeds of FtsW-RFP in superfission variant  $ftsB^{E56A}$   
404 (orange), WT (grey),  $ftsB^{E56A} \Delta ftsN$  (yellow), and FtsN-depleted (blue) cells. **c.** CDF (circles) of  
405 histograms in **b** and the corresponding best fits (solid curves).

406

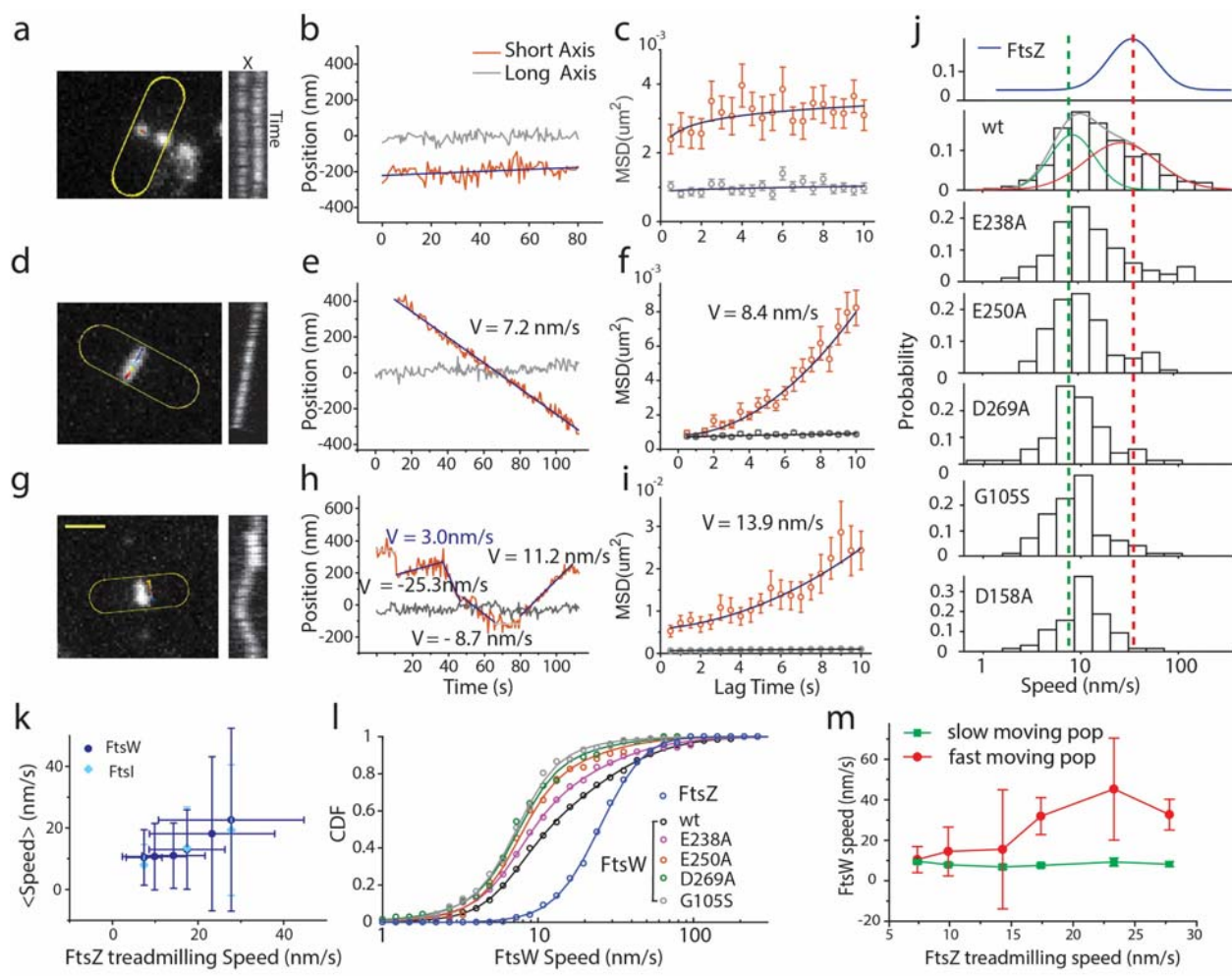
407 **Figure 5. A two-track model integrating spatial information into the regulation of sPG synthase**  
408 **activity. a.** Summary plot showing that when sPG synthesis activity is inhibited the average speeds of all  
409 directional moving FtsW molecules increases due to the increased fraction of the fast-moving, inactive  
410 FtsW population; conversely, when sPG synthesis activity is enhanced, the average speed of FtsW  
411 decreases due to the increased fraction of the slow-moving, active FtsW population. **b.** A two-track model  
412 depicting that when the synthase FtsWI complex follows the treadmilling FtsZ track it remains inactive  
413 but becomes active on the sPG track once it exits the Z-track. FtsN plays an important role in promoting  
414 the release of FtsWI from the Z-track to pursue sPG synthesis on the sPG track.

415 **Fig 1**



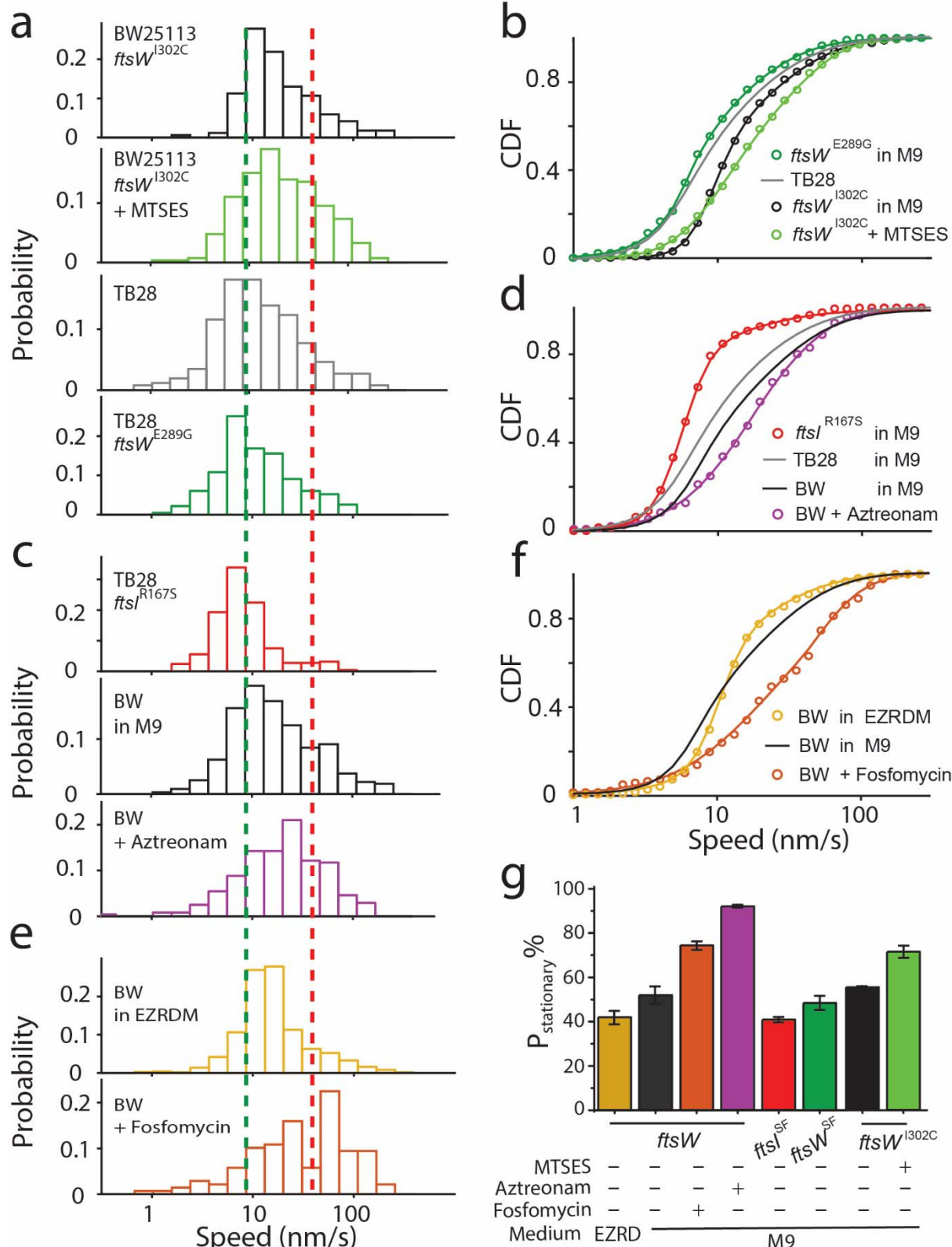
417

418 Fig 2



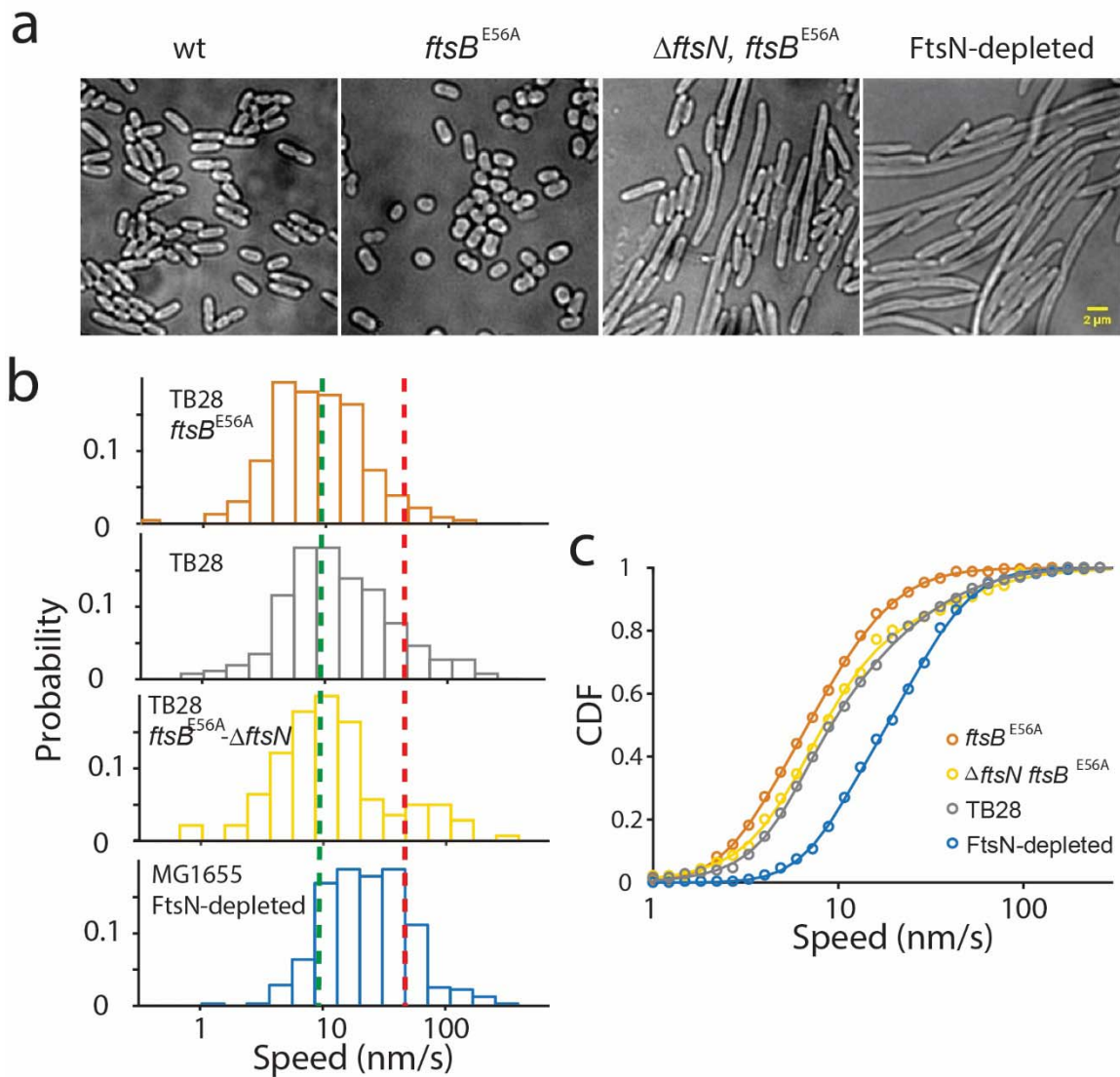
419

420 Fig 3



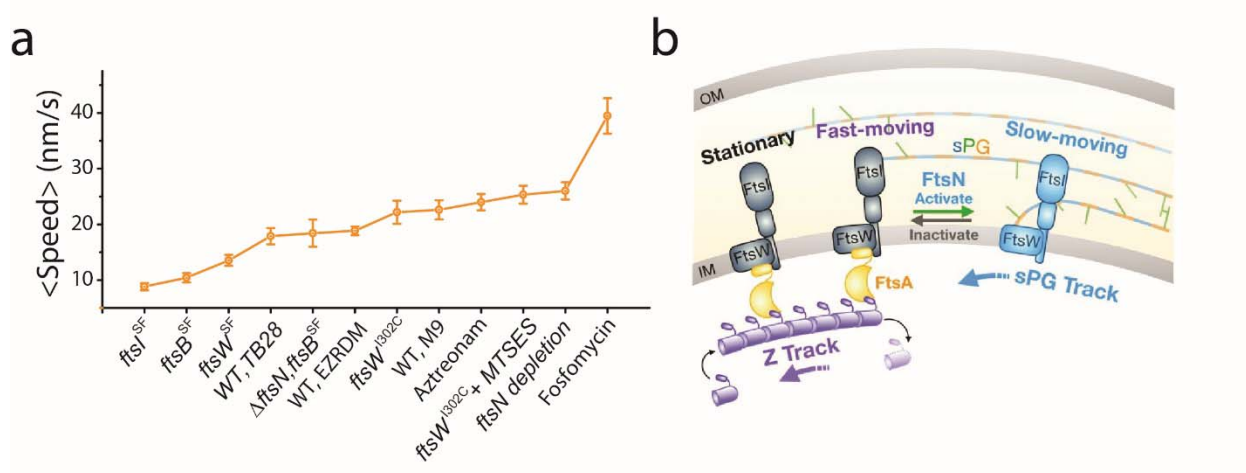
421

422 **Fig 4**



423

424 **Fig 5**



425